Journal of Power Sources 207 (2012) 199–204

Contents lists available at SciVerse ScienceDirect

Journal of Power Sources

journal homepage: www.elsevier.com/locate/jpowsour

# In situ construction of potato starch based carbon nanofiber/activated carbon hybrid structure for high-performance electrical double layer capacitor

Qianqian Li[a], Fu Liu[a,*], Li Zhang[b,*], Bradley J. Nelson[b], Sihan Zhang[a], Chao Ma[a], Xinyong Tao[c], Jipeng Cheng[a], Xiaobin Zhang[a]

[a] Department of Materials Science and Engineering, State Key Laboratory of Silicon Materials, Zhejiang University, Hangzhou 310027, China
[b] Institute of Robotics and Intelligent Systems, ETH Zurich, CH-8092 Zurich, Switzerland
[c] College of Chemical Engineering and Materials Science, Zhejiang University of Technology, Hangzhou 310027, China

ARTICLE INFO

*Article history:*
Received 7 November 2011
Received in revised form 15 January 2012
Accepted 26 January 2012
Available online 3 February 2012

*Keywords:*
Potato starch
Activated carbon
Carbon nanofibers
Electrochemical capacitor

ABSTRACT

Hybrid structures of carbon nanofibers (CNFs) and activated carbon (AC) have been fabricated using natural potato starch as the substrate for in situ growth of the CNFs. Iron nitrate was used as both the activation agent and the catalyst precursor. The AC was derived from potato starch and the CNFs grew from the surface of AC. The hybrid structure has a large specific surface area (approximately 1930 $m^2 g^{-1}$) and exhibits excellent electrochemical properties as supercapacitor for electrode materials. Its capacitance reaches a peak value of 268 $F g^{-1}$ with an excellent cyclical ability, which is attributed to the unique hybrid structure, large specific surface area, and the high electron conductivity of CNFs grown in situ with AC. These low cost, eco-friendly CNF/AC hybrid structures are promising for energy storage.



## 1. Introduction

Electrochemical capacitors, also known as supercapacitors or ultracapacitors, have a specific energy several orders of magnitude higher than conventional ones [1–3] Due to their long cycle life, high cycle efficiency and high power density, they have potential applications in electric vehicles, cold or heavy-load starting assists, utility load leveling, low-frequency smoothing of power supplies, and military and medical devices [4]. Among various electrode materials used for supercapacitors, carbon-related materials are mainly based on the accumulation of charges in an electrical double layer without faradic reaction [5]. Activated carbon (AC) is one of the most frequently used electrode materials in electrochemical capacitors because of its low cost, high surface area, and well established production technologies [6–8]. Though AC has been widely studied in the past decades, the inherent poor electrical conductivity and low capacitance retention rate at high charge–discharge rate are still the drawback of the AC electrode; in addition, the preparation processes are still sophisticated, time and energy consuming, and non-renewable raw materials are mainly used. On the other hand, carbon nanofibers (CNFs), used for the electrodes of electrochemical capacitors [9–11], have also been studied for several years because of their excellent mechanical performance and good electrical and thermal conductivity. In addition, one-dimensional CNFs can provide a network structure that combines low electrical resistivity and high porosity of materials, similar to AC. It is also considered to be an excellent substitute in electrodes to replace acetylene black [12].

Using agricultural byproducts and natural plant resources as precursors for preparing AC is promising [13–16] because the materials are cheap, abundant and eco-friendly [17,18]. We report an approach to synthesize nanocomposites of CNFs and AC (CNF/AC), where the AC was derived from potato starch and CNFs were grown in situ on the surface of as-prepared AC by chemical vapor deposition (CVD). The formation of the catalyst to grow CNFs was analyzed and the effects of network structure on the enhanced electrochemical performance were investigated and compared to electrodes prepared from mechanically mixed CNFs and pure AC, where the CNFs were grown by CVD, and the AC was derived from potato starch. The results indicate that the nanocomposites have excellent electrochemical performance and strong potential for energy storage applications.

## 2. Experimental

### 2.1. Carbon material preparation

The procedure to synthesize CNF/AC nanocomposites is shown in Fig. 1. (I) Preparation of potato starch and iron nitrate mixture: 1 g potato starch was impregnated with 25 ml appropriate

* Corresponding authors. Tel.: +86 571 879 51411; fax: +86 571 879 51411.
*E-mail addresses:* liufu@zju.edu.cn (F. Liu), lizhang@ethz.ch (L. Zhang).

0378-7753/$ – see front matter © 2012 Elsevier B.V. All rights reserved.
doi:10.1016/j.jpowsour.2012.01.142

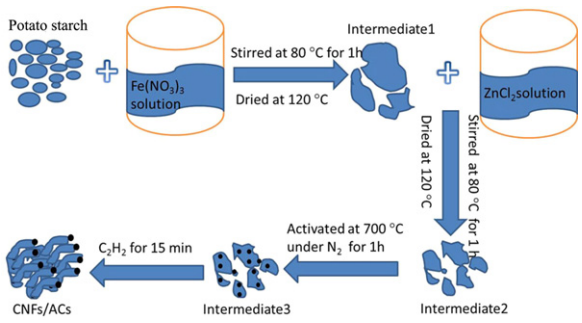


**Fig. 1.** Schematic illustration depicts the preparation of CNF/AC nanocomposites.

concentration aqueous solution of $Fe(NO_3)_3$ (see Table 1), stirred at room temperature for 1 h, and then the solvent was evaporated at 80 °C and further dried at 120 °C to obtain intermediate "1". (II) Activation: 1 g intermediate "1" was added to 25 ml of 60 wt.% $ZnCl_2$ aqueous solution [19,20], stirred at 80 °C for 1 h, and dried at 120 °C overnight obtaining intermediate "2". The activation process was carried out by keeping the intermediate "2" at 700 °C in a quartz tube reactor for 1 h under a $N_2$ atmosphere to obtain intermediate "3". (III) In situ growth of CNFs: acetylene was introduced into the quartz tube reactor, where intermediate "3" was placed after step II, for 15 min and then cooled to room temperature. The product was mixed with hydrochloric acid, boiled for 1 h, thoroughly washed with distilled water until neutral, and then dried. In this procedure the mass ratio of potato starch to iron nitrate was tuned in order to improve electrochemical performance.

For comparison of the electrochemical performance with the samples of in situ grown CNF/AC, CNFs separately synthesized by CVD [21] and then mechanically mixed with AC prepared from potato starch as the electrode material (see sample 1 in Table 1) were conducted.

### 2.2. Nanocomposite characterization

The crystalline properties of samples were characterized by X-ray diffraction (XRD, X'Pert PRO) over a range of 2° from 10° to 80° with a step size of 0.02°. Thermal gravimeter-differential scanning calorimeter (TG-DSC) measurements were performed by thermal analysis (DSCQ1000, AT, America). The mixture of starch and iron nitrate as well as pure starch was investigated by TG-DSC to determine phase transformations. The temperature was raised from 20 °C to 800 °C in a nitrogen atmosphere. Morphologies and structures of products were analyzed by scanning electron microscopy (SEM, Hitachi S-4800) and transmission electron microscopy (TEM, Philips CM-200). Specific surface areas of the prepared nanocomposites and the as-prepared AC were determined by the Brunauer–Emmentt–Teller (BET) method.

### 2.3. Preparation of electrodes

The supercapacitor electrodes for electrochemical measurement were prepared by mixing the carbon materials with polyvinylidene fluoride (PVDF) as binders. They were mixed in a weight ratio of 80:20 in the N-methyl-2-pyrrolidone (NMP) solvent, and then painted on the surface of nickel foam plates (1 cm × 1 cm). The active material loaded on the electrode was approximately 8 mg on each electrode. The two prepared electrodes were separated by a polypropylene film, tightly fixed by double plexiglass plates as a prototype supercapacitor, and fully wetted with 6 M KOH electrolyte. Four samples were prepared as the electrode materials as shown in Table 1.

**Table 1**
Composites and the specific capacitance of all the samples.

| Sample No. | 1 | 2 | 3 | 4 |
|---|---|---|---|---|
| Component[a] | AC mixed with CNF | 1:1 | 5:1 | 10:1 |
| Result 1[b] ($F g^{-1}$) | 63 | 132 | 251 | 177 |
| Result 2[c] ($F g^{-1}$) | 67 | 120 | 268 | 181 |

[a] Ratio of potato starch to iron nitrate for samples 2–4.
[b] The specific capacitance calculated by CV curves.
[c] The specific capacitance calculated by discharge curves.

### 2.4. Electrochemical measurements

Cyclic voltammetry (CV) was conducted on an electrochemical work station (CHI660B). The voltage range in the CV test was 0–1 V with a scan rate of 10 mV $s^{-1}$. The galvanostatic charge–discharge was performed on a software-controlled battery test system (PCBT-B8-8D-A) operated at a current density of 500 mA $g^{-1}$ in a potential range from 0.01 to 1 V. All electrochemical measurements were carried out using 6 M KOH as the electrolyte solution at room temperature. The specific gravimetric capacitance was calculated from the CV curves according to:

$$C_g = \int \frac{idV}{\nu m \Delta V} \quad (1)$$

or from the discharge process of the third cycle in a potential range of 0.2–0.8 V according to:

$$C_g = \frac{2i\Delta t}{m\Delta V} \quad (2)$$

where $C_g$ ($F g^{-1}$) is the mass-specific gravimetric capacitance; $i$ (A) is the current; $\Delta t$ (s) is the change of the negative process duration in the evaluated region; $\Delta V$ (V) is the potential change during the discharge process; $\nu$ is the potential scan rate (mV $s^{-1}$); and $m$ (g) is the mass of activated materials in the electrode.

## 3. Results and discussion

Fig. 2a and b demonstrates the morphologies of pure potato starch and intermediate "1". Pure potato starch exhibited potato-like balls with an average diameter of 20 μm and a smooth surface (see Fig. 2a). The morphology transformed into polyhedron-like shapes with a rough surface of intermediate "1", as shown in Fig. 2b. The impregnation process resulted in severe agglomeration and sintering of the starch. However, there are not pores on the surface of intermediate "1". After activation by zinc chloride a large number of small pores appeared on the rough surface as shown in Fig. 2c. CNFs in situ grown on the surface of AC are shown in Fig. 2d. The diameters of CNFs are in the range of 30–170 nm, and the average diameter of CNFs is approximately 80 nm. In Fig. 2e, the TEM image of CNF/AC reveals that CNFs are grown from many catalyst particles that root on the surface of AC, indicating the top growth mechanism. In Fig. 2f, a high-resolution TEM image indicates that CNFs with a regular lattice spacing of 0.34 nm corresponds to the (0 0 2) interplanar distance of graphite structure.

Fig. 3a and b shows thermogravimetric (TG) and differential scanning calorimetry (DSC) diagrams of pure potato starch and starch impregnated with 50 wt.% iron nitrate solution, respectively. In Fig. 3a, an endothermic peak (83 °C) in the DSC curve indicates the gelatinization behavior of potato starch [22] corresponding to the evolution of moisture in which the content fraction of water is about 20 wt.%. The next endothermic peak (290 °C) is attributed to the thermal decomposition of potato starch [23], showing that potato starch was carbonized at about 300 °C. The TG-DSC curve of potato starch impregnated with iron nitrate, shown in Fig. 3b, is more complicated than the curve in Fig. 3a, which has two more endothermic peaks compared to Fig. 3a. The formation process of

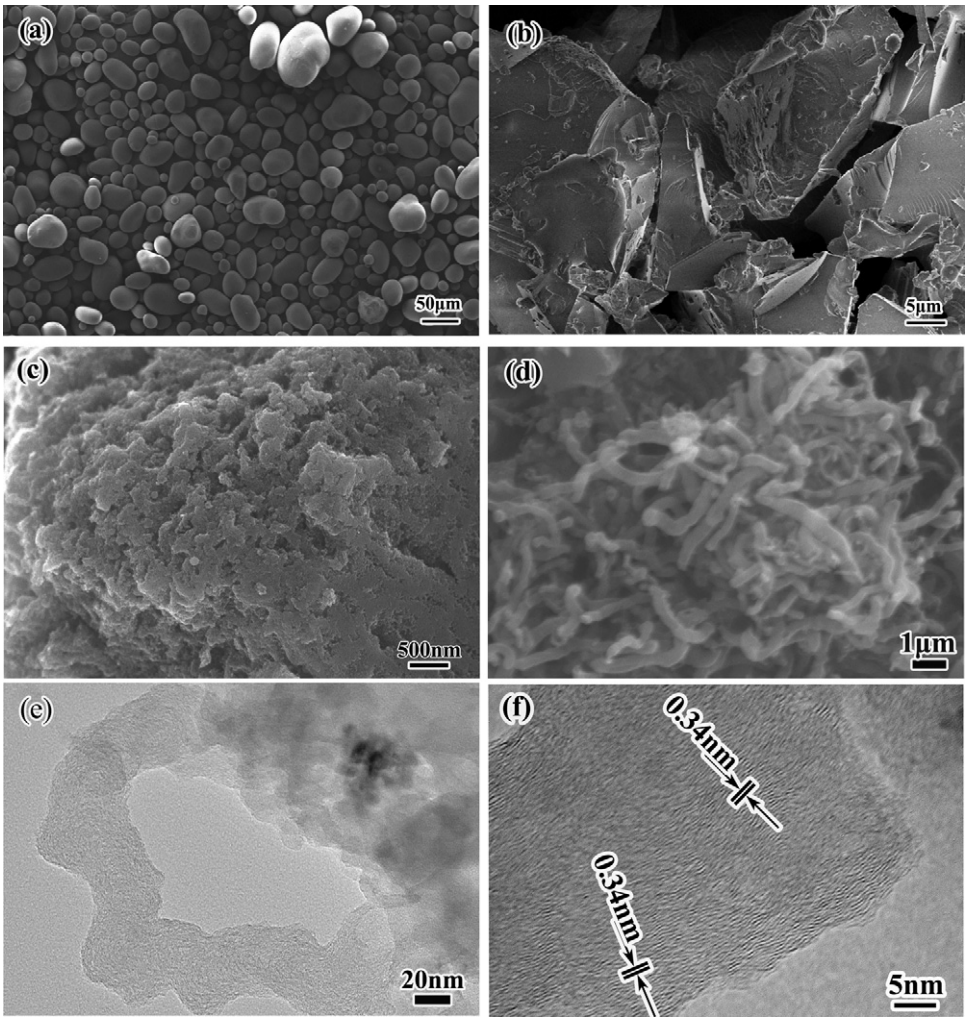


**Fig. 2.** SEM micrograph of (a) pure potato starch; of (b) intermediate "1", of (c) pure AC and of (d) CNF/AC nanocomposite for sample 3, (e) TEM micrograph of CNF/AC nanocomposite, and (f) high resolution TEM micrograph of CNF/AC nanocomposite.

catalyst for CNFs can be deduced from Fig. 3b. The first endothermic peak drifted to a lower temperature (77 °C) due to the decomposition of iron nitrate which also accelerated the meltdown of starch particles. The second endothermic peak (194 °C) represents the initial decomposition of iron nitrate with $HNO_3$ and the release of $NO_x$ [24]. The exothermal peak (295 °C) between the second endothermic peak and the third is due to gas–solid reactions occurring simultaneously with the decomposition of potato starch. $HNO_3$ and $NO_x$ are strong carbon oxidants with CO and $CO_2$ as byproducts. Though potato starch decomposition is endothermic, the net effect can be exothermic depending on the extent of the oxidation [25]. Introduction of iron nitrate results in more gas release producing more pores in the AC. The third endothermic peak (390 °C) is the decomposition of hydroxynitrate releasing Fe oxides, $HNO_3$, $NO_x$ and water [26]. The reduction of iron oxides by carbon atoms corresponds to the last endothermic peak (588 °C).

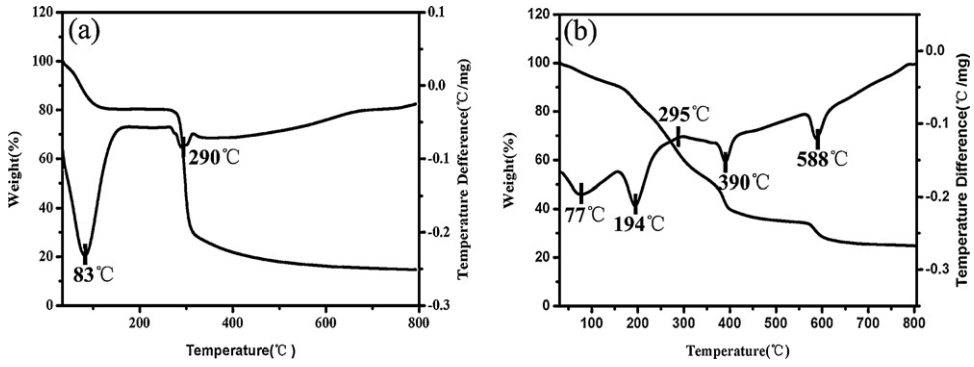


**Fig. 3.** TG-DSC diagrams: (a) pure potato starch; (b) potato starch impregnated in iron nitrate with the ratio of 1:1.

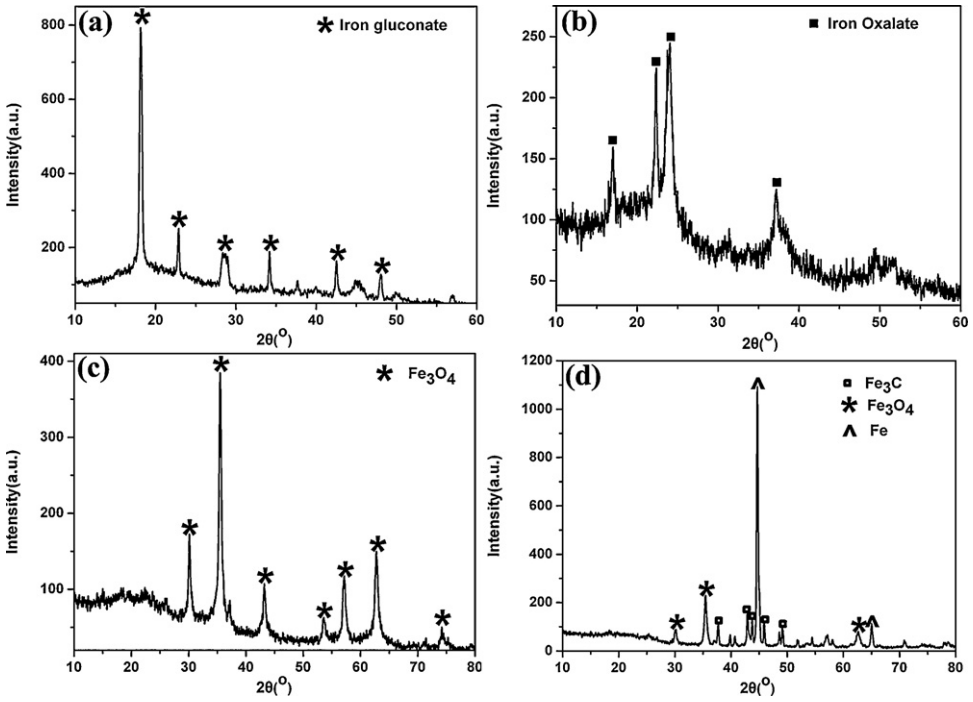


**Fig. 4.** XRD patterns of the potato starch and iron nitrate composite heated at (a) 200 °C, (b) 300 °C, (c) 400 °C and (d) 600 °C.

Fig. 4a–d shows XRD patterns to investigate the catalyst forming process. The samples of potato starch and iron nitrate mixture for XRD examinations were heated for 1 h at 200 °C, 300 °C, 400 °C and 600 °C, respectively, corresponding to the weight loss, the endothermic and exothermic stages at the same temperatures displayed on the TG-DSC (Fig. 3b). The XRD pattern of Fig. 4a shows pure iron gluconate (JCDS NO. 05-0257) formed after the drying of the mixture in the first heating stage at 200 °C. By increasing the temperature to 300 °C, iron gluconate reacted with $HNO_3$ (generated from iron nitrate and potato starch decomposition), then iron oxalate (JCDS NO. 17-0807), shown in Fig. 4b, formed by the gas–solid reaction associated with heat release [25]. Pure $Fe_3O_4$ (JCDS NO. 65-3170) phase was formed as the temperature reached the next endothermic peak at 400 °C as shown in Fig. 4c. When the sample was heated to 600 °C, as showed in Fig. 4d, the phase of Fe (JCDS NO. 06-0696) and $Fe_3C$ (JCDS NO. 72-1110) were also detected. $Fe_3O_4$ was reduced by carbon atoms. Simultaneously partial iron and carbon reacted and formed a compound of $Fe_3C$ [27], which acts as a catalyst for in situ CVD growth of CNFs in the subsequent process. Fig. 5 shows the synthesis flow chart of the catalysts from potato starch and iron nitrate resulting from the XRD analysis (see in Fig. 4).

Iron nitrate was used as the activation agent and the catalyst precursor. The iron addition has three effects: (1) the degradation of iron nitrate plays an important role in carbonization of the potato mash and makes the preparation of the nanocomposites straightforward, time efficient and low cost; (2) iron nitrate can act as activation agent for the second activation of AC. Thermolysis of nitrates can produce nitric oxide and iron oxide, which can activate the AC again; (3) Fe and $Fe_3C$ resulted from the reduction of iron oxides can act as the catalyst for the in situ growth of CNFs on AC.

The nitrogen adsorption–desorption isotherms and pore size distributions were used to characterize the porous structure of CNF/AC nanocomposite and pure AC, as shown in Fig. 6. Fig. 6a and b shows the adsorption and desorption curves and the distribution of pore sizes, respectively. The nitrogen adsorption–desorption plots shown in Fig. 6a can be classified as type IV, i.e. a typical mesoporous character according to IUPAC. The adsorption of $N_2$ is observed at a relatively low pressure ($P/P_0 < 0.02$) due to the micropore-filling effect. Adsorption gradually increases in the region of middle $P/P_0$ and further in the region of high pressure (>0.5 $P/P_0$). Such an adsorption behavior can be attributed to the capillary condensation of nitrogen in the mesopores and multilayer adsorption of mesopores. Fig. 6b shows that the pore sizes of pure AC distribute in 2–3 nm and 3–4 nm, which has a high BET surface area of 2086 $m^2\ g^{-1}$ and a total pore volume of 2.4 $cm^3\ g^{-1}$. The higher the surface area of carbon supports, the more deposition sites for the catalyst particles [28]. After the growth of CNFs on the AC, the BET surface area slightly decreased to 1930 $m^2\ g^{-1}$, and the total pore volume decreased to 2.3 $cm^3\ g^{-1}$. Since the catalysts can be deposited on the pores more easily, the CNFs have the opportunity to grow in the sites where the catalysts lie.

The electrochemical impedance spectroscopy (EIS) is employed to monitor the electrochemical behavior of the electrodes. Nyquist plots for analyzing the capacitance behavior of all samples, collected in the frequency range of 100 kHz–1 mHz, are shown in Fig. 7.

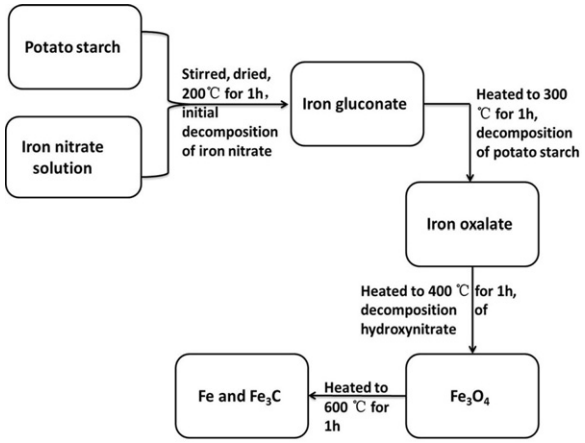


**Fig. 5.** Synthesis flow chart of the catalysts from potato starch and iron nitrate.

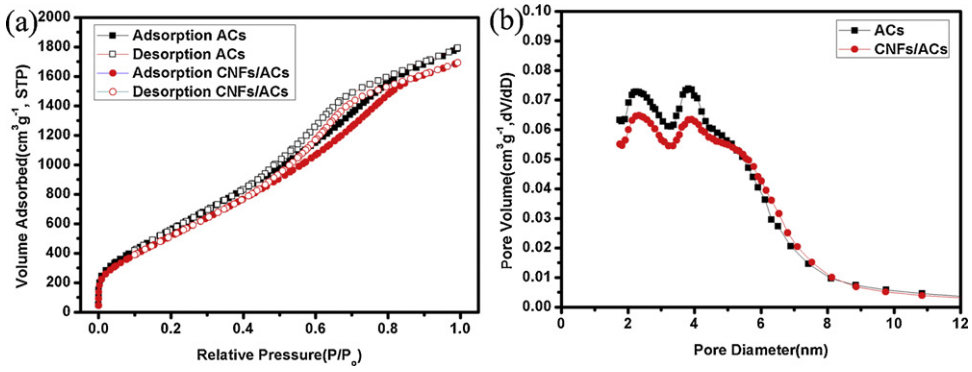


**Fig. 6.** (a) The $N_2$ adsorption isotherms; and (b) the Barrett–Joyner–Halenda (BJH) pore size distributions of AC and CNF/AC nanocomposite with a mass ratio of potato and iron nitrate 5:1.

The enlarged high-frequency region of the impedance spectra can be seen more clearly. Generally speaking, all spectra are similar in shape, where in the high frequency region there is a semicircle that is indicative of contact resistance [29–31]. In the low frequency region, a nearly vertical line demonstrates the domination of capacitive behavior at the electrolyte/electrode material interface. Fig. 7 shows that sample 3 has the best performance among all the samples. On contrast, the resistance of the electrode made of sample 4 is higher than others due to the diffusion limits of electrolyte ions of the little quantity of CNFs. Fig. S4 shows when the mass ratio between potato starch and iron nitrate for sample 4 is 10:1, the CNF nearly disappeared. It is because so little quantity of iron addition acted as catalyst for the growth of CNF, then only the short beard-like carbon material grew on the AC surface. When the mass ratio of potato starch to iron nitrate is 5:1 (sample 3), the resistance reaches a minimum. The better electrical conductivity is understood that the CNFs grown in situ with AC (see Fig. 2d) can form a conductive network and lower the resistance. The advantage of in situ grown CNF/AC composite also is noticed on comparison with sample 1 with much larger resistance, in which the CNFs were mechanically incorporated. Moreover, the CNF/AC composite is favorable for ions to transport in the KOH aqueous electrolyte.

Typical cyclic voltammograms (CV) were conducted at a scan rate of 10 mV $s^{-1}$ with a potential range of 0–1 V as shown in Fig. 8. All CV curves have rectangular shapes. However, the rectangular shapes of sample 3 and sample 4 exhibited a slightly distorted, which may be due to diffusion limited capacitance [32]. The CV curve of sample 3 exhibits larger area of the loop, demonstrating it has higher specific capacitance. Specific capacitances of all the samples can be calculated from Eq. (1). It gives the largest specific capacitance of 251 F $g^{-1}$ for sample 3, and others are 177 F $g^{-1}$ (sample 4), 132 F $g^{-1}$ (sample 2) and 63 F $g^{-1}$ (sample 1), respectively, according to Fig. 8. Although sample 4 showed high resistance its capacitance is still hold on large because of relatively large BET surface (1846 $m^2$ $g^{-1}$).

To investigate the stability of the electrodes, typical galvanostatic charge–discharge curves were obtained for the four samples at a constant current density of 500 mA $g^{-1}$ and a potential range from 0.01 to 1 V (Fig. 9a). The approximate linear charge–discharge curve corresponds to that of an ideal electrochemical capacitor. The approximately symmetric triangles indicate that the circulation property of the supercapacitors is excellent. The values of specific capacitance can also be calculated from the discharge curves from Eq. (2), in which the specific capacitance of sample 1–4 is 67 F $g^{-1}$, 120 F $g^{-1}$, 268 F $g^{-1}$ and 181 F $g^{-1}$, respectively. Thus, sample 3 exhibits the highest specific capacitance which is 13% higher than previous report [17]. Though the BET surface area of pure AC is higher than that of CNF/AC, the specific capacitance of CNF/AC is approximately four times higher than that of pure AC. The CNFs in situ grown on AC show good conductivity and can store charges with the substrate AC. To investigate the contribution of CNFs to the total capacitance, we tested the electrode made of AC without CNFs, and the resulted specific capacitance is only 96 F $g^{-1}$, though the BET surface area of AC is as large as 2086 $m^2$ $g^{-1}$. It is probably that the pores in the AC were not fully utilized due to the absence of CNFs. The dependence of specific capacitance of electrodes on the current density is shown in Fig. 9b. There is no obvious

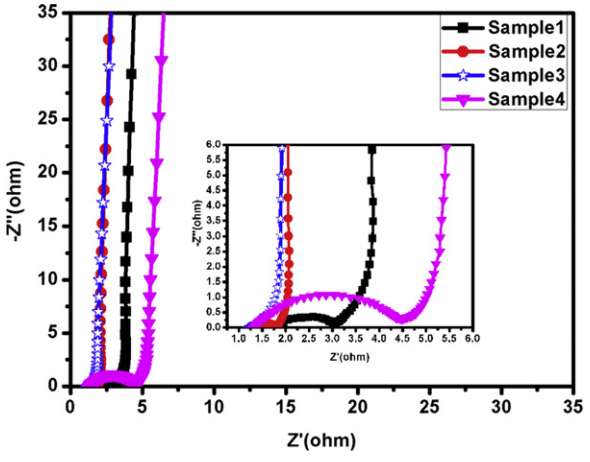


**Fig. 7.** Nyquist plots for all the samples in 6 M KOH at frequencies of 1 mHz–100 kHz. The inset shows the magnification of the high-frequency region of the impedance spectra.

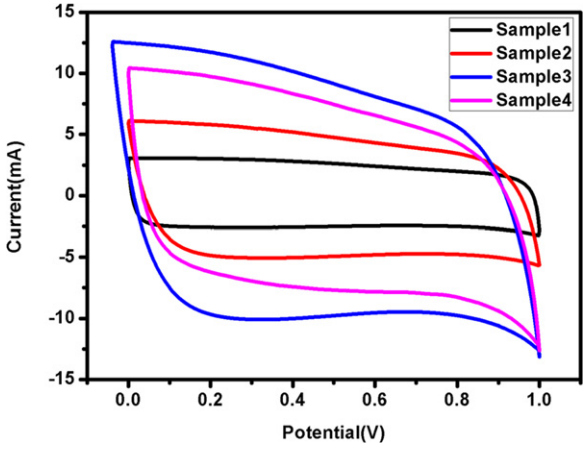


**Fig. 8.** Cyclic voltammograms of the supercapacitors based on the four samples, sweep rate is 10 mV $s^{-1}$, potential range is 0–1 V.

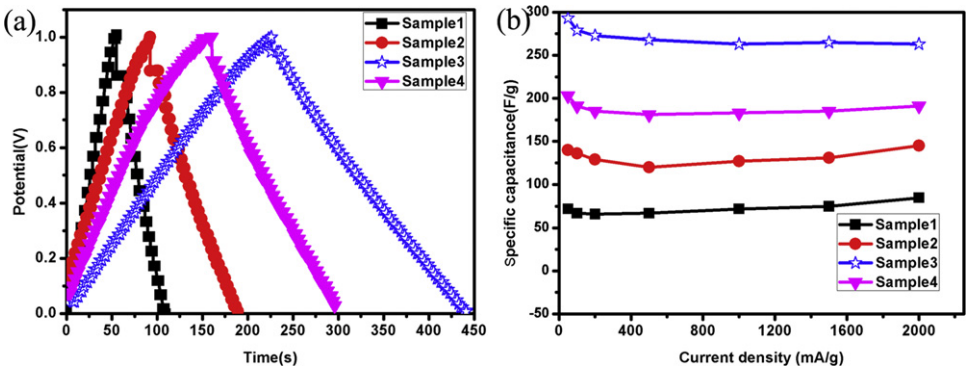


**Fig. 9.** The galvanostatic charge–discharge curves at current density of 500 mA $g^{-1}$ and (b) the specific capacitance at various current densities for all the samples.

change at both low and high current density. The better capacitive performance of CNF/AC nanocomposite electrodes than that of the electrode made by mixed AC with CNFs can be attributed to the low resistance and porosity of the structure. The decrease of the specific capacitance of all the samples are negligible with a current density up to 2000 mA $g^{-1}$, which implies that the electrode is stable and the charge–discharge process is reversible.

## 4. Conclusions

Activated carbon was prepared from potato starch by activation with $ZnCl_2$. CNF/AC composites were directly synthesized using the CVD method with Fe and $Fe_3C$ as a catalyst. The introduction of iron nitrate plays an important role in carbonization, and it makes the preparation of the nanocomposites straightforward, time efficient and low cost. When the mass ratio of potato starch to iron nitrate is 5:1, the highest capacitance reaches 268 F $g^{-1}$ with excellent circulation and stability, which is attributed to the unique structural properties of the composite including the large surface of the base AC, the high electron conductivity of CNFs grown in situ with AC, and the larger range of pore size distribution of the composite. CNF/AC nanocomposites prepared by this method are a promising material as an electrode for supercapacitors.

## Acknowledgements

This work was financial supported by the Zhejiang Province Natural Science Foundation (Y4080129), Zhejiang Province Environmental Protection Science Research Plan (2011B14), the Opening Foundation of Zhejiang Provincial Top Key Discipline (No. 20110905), and the Sino-Swiss Science and Technology Cooperation (SSSTC, Grant No. EG 08-092009).

## Appendix A. Supplementary data

Supplementary data associated with this article can be found, in the online version, at doi:10.1016/j.jpowsour.2012.01.142.

## References

[1] Y.D. Zhu, H.Q. Hu, W.C. Li, X.Y. Zhang, Carbon 45 (2007) 160–165.
[2] C. Schmitt, H. Probstle, J. Fricke, Journal of Non-Crystalline Solids 285 (2001) 277–282.
[3] S. Nohara, H. Wada, N. Furukawa, H. Inoue, M. Morita, C. Iwakura, Electrochimica Acta 48 (2003) 749–753.
[4] B.E. Conway, Electrochemical supercapacitors: Scientific Fundamentals and Technological Applications, Kluwer Academic/Plenum Publishers, New York, 1999.
[5] A. Chu, P. Braatz, Journal of Power Sources 112 (2002) 236–246.
[6] Y.D. Zhu, H.Q. Hu, W.C. Li, X.Y. Zhang, Journal of Power Sources 162 (2006) 738–742.
[7] Y.H. Wen, G.P. Cao, Y.S. Yang, Journal of Power Sources 148 (2005) 121–128.
[8] L. Zhang, H.B. Liu, M. Wang, L. Chen, Carbon 45 (2007) 1439–1445.
[9] C. Kim, K.S. Yang, Applied Physics Letters 83 (2003) 1216–1218.
[10] J. Jang, J. Bae, M. Choi, S.H. Yoon, Carbon 43 (2005) 2730–2736.
[11] K. Naoi, S. Ishimoto, Y. Isobe, S. Aoyagi, Journal of Power Sources 195 (2010) 6250–6254.
[12] M. Lake, in: L.P. Biró, C.A. Bernardo, G.G. Tibbetts, Ph. Lambin (Eds.), Carbon Filaments and Nanotubes: Common Origins, Differing Applications?, Kluwer Academic Publishers, Dordrecht, 2001.
[13] M.S. Balathanigaimani, W.G. Shim, M.J. Lee, C. Kim, J.W. Lee, H. Moon, Electrochemistry Communications 10 (2008) 868–871.
[14] C.C. Hu, C.C. Wang, F.C. Wu, R.L. Tseng, Electrochimica Acta 52 (2007) 2498–2505.
[15] F.C. Wu, R.L. Tseng, C.C. Hu, C.C. Wang, Journal of Power Sources 144 (2005) 302–309.
[16] Y.J. Kim, B.J. Lee, H. Suezaki, T. Chino, Y. Abe, T. Yanagiura, K.C. Park, M. Endo, Carbon 44 (2006) 1592–1595.
[17] H.Q. Wang, Y.L. Zhong, Q.Y. Li, J.H. Yang, Q.F. Dai, Journal of Physics and Chemistry of Solids 69 (2008) 2420–2425.
[18] S. Zhao, C.Y. Wang, M.M. Chen, J. Wang, Z.Q. Shi, Journal of Physics and Chemistry of Solids 70 (2009) 1256–1260.
[19] N.R. Khalili, M. Campbell, G. Sandi, J. Golas, Carbon 38 (2000) 1905–1915.
[20] K. Mohanty, D. Das, M.N. Biswas, Chemical Engineering Journal 115 (2005) 121–131.
[21] J.P. Cheng, X.B. Zhang, F. Liu, J.P. Tu, H.M. Lu, Y.L. Sun, F. Chen, Materials Chemistry and Physics 87 (2004) 241–245.
[22] H.S. Liu, L. Yu, G. Simon, K. Dean, L. Chen, Carbohydrate Polymers 77 (2009) 662–669.
[23] S. Zhao, C.Y. Wang, M.M. Chen, J.H. Sun, Carbon 47 (2009) 331–333.
[24] A. Malecki, R. Gajerski, S. Labus, B. Prochowska-Klisch, K.T. Wojciechowski, Journal of Thermal Analysis and Calorimetry 60 (2000) 17–23.
[25] L.M.S. Silva, J.J.M. Orfao, J.L. Figueiredo, Applied Catalysis A-General 209 (2001) 145–154.
[26] C. Jia, Y. Cheng, F. Bao, D.Q. Chen, Y.S. Wang, Journal of Crystal Growth 294 (2006) 353–357.
[27] I.F. Silva, D.W. McKee, L.S. Lobo, Journal of Catalysis 170 (1997) 54–61.
[28] P.L. Kuo, C.H. Hsu, W.T. Li, J.Y. Jhan, W.F. Chen, Journal of Power Sources 195 (2010) 7983–7990.
[29] B.Z. Fang, L. Binder, Journal of Physical Chemistry B 110 (2006) 7877–7882.
[30] W.J. Lee, Y.W. Ju, G.R. Choi, H.R. Jung, Electrochimica Acta 53 (2008) 5796–5803.
[31] Y.H. Lee, K.H. An, W.S. Kim, Y.S. Park, Y.C. Choi, S.M. Lee, D.C. Chung, D.J. Bae, S.C. Lim, Advanced Materials 13 (2001) 497–500.
[32] M.R. Jisha, Y.J. Hwang, J.S. Shin, K.S. Nahm, T.P. Kumar, K. Karthikeyan, N. Dhanikaivelu, D. Kalpana, N.G. Renganathan, A.M. Stephan, Materials Chemistry and Physics 115 (2009) 33–39.